



# PCCP

## Direct Observation of $C_{60}^-$ Nano-ion Gas Phase Ozonation via Ion Mobility-Mass Spectrometry

|                               |   |
|-------------------------------|---|
| Journal:                      | <i>Physical Chemistry Chemical Physics</i>  |
| Manuscript ID                 | CP-ART-03-2019-001394.R1  |
| Article Type:                 | Paper   |
| Date Submitted by the Author: | 20-Apr-2019   |
| Complete List of Authors:     | Li, Chenxi; ETH Zürich, Dep. of Chemistry and Applied Biosc.<br>Hogan Jr., Christopher; University of Minnesota Twin Cities, Mechanical Engineering |
|                               |   |

SCHOLARONE™  
Manuscripts

# **Direct Observation of $C_{60}^-$ Nano-ion Gas Phase Ozonation via Ion Mobility-Mass Spectrometry**

Chenxi Li<sup>1,2</sup>, Christopher J. Hogan Jr<sup>1\*</sup>

<sup>1</sup>Department of Mechanical Engineering, University of Minnesota, Minneapolis, MN 55455, USA

<sup>2</sup>Laboratory for Physical Chemistry, ETH Zürich, 8093 Zürich, Switzerland

**Submitted to:**

**Physical Chemistry Chemical Physics**

\*To whom correspondence should be addressed: [hogan108@umn.edu](mailto:hogan108@umn.edu), T: 1-612-626-8312

**ABSTRACT**

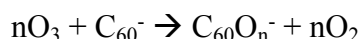
Improved methods to probe the reactivity of nano-ions, such as  $C_{60}^-$ , would find utility in nanochemistry, combustion chemistry, and in generally understanding the behavior of matter at the nanometer scale. We demonstrate that ion mobility-mass spectrometry (IM-MS) with a low-field differential mobility analyzer can be used to probe nano-ion reaction kinetics. We developed IM-MS approach to examine the gas phase reactivity of  $C_{60}^-$  ions with ozone at atmospheric pressure. Experimental results show that ozonation of  $C_{60}^-$  mainly leads the formation of  $C_{60}O_n^-$ . The controlled reaction time within the ion mobility instrument enables calculation of ozonation reaction rates and assuming oxygen atoms are added sequentially, we find that the reaction rate between  $C_{60}^-$  and  $O_3$  is near the collision controlled limit. We propose an exponentially decaying reaction rate coefficient expression to describe ozonation leading to the addition of  $>20$  oxygen atoms. At high ozone concentrations, CO or  $CO_2$  loss from  $C_{60}O_n^-$  is additionally observed.

## INTRODUCTION

Since its initial discovery, the reactivity of  $C_{60}$  has been the focus of a number of studies, including but not limited to studies of  $C_{60}$  polymerization,<sup>1, 2</sup> derivatization,<sup>3-5</sup> and ozone induced oxidation<sup>6-9</sup> (ozonation). While earlier studies (several decades ago) detailed cationic  $C_{60}$  gas phase reactions,<sup>10-13</sup> and  $C_{60}$  gas phase aggregation,<sup>14, 15</sup> recent  $C_{60}$  reactivity studies have focused solely on condensed phase reactivity, including in films or for  $C_{60}$  suspended in solvent. There is presently limited research probing the reactivity of gas phase  $C_{60}^-$  nano-ions, i.e. isolated  $C_{60}$  molecules in the gas phase ionized by electron addition. Further study of the reactivity of nano-ions is nonetheless of considerable interest; reactions with the ordered graphene  $C_{60}^-$  structure may serve to inform the behavior of other graphene based materials, soot precursors,<sup>16, 17</sup> and nanometer scale inorganic carbonaceous material.<sup>18</sup> More generally, such studies would help to better understand the properties of nanometer scale species,<sup>19</sup> whose behavior is often distinct from bulk material,<sup>20, 21</sup> as they lie between the small molecule and nanoparticle limits of gas phase reaction behavior.

There is hence continued reason to develop methods to probe reaction kinetics of gas phase fullerene nano-ions. Here, we show how recent advances in instrumentation used for ion mobility-mass spectrometry (IM-MS) enable examination of gas phase nano-ion chemistry. In the past decade, a variety of drift tube,<sup>22-24</sup> differential mobility analyzer (DMA),<sup>25</sup> traveling wave,<sup>26</sup> and trapped mobility<sup>27</sup> instruments have been developed, enabling modest to high resolution characterization of nano-ion structures. Though such instruments have largely been utilized in two-dimensional separations of biomolecules,<sup>28</sup> or to probe the gas phase conformational space of non-covalently bound complexes,<sup>29</sup> control over the bath gas composition<sup>30, 31</sup> and residence time within ion mobility systems also facilitate studies of ion

chemistry; recent studies have shown that binding free energies can be inferred using IM-MS measurements,<sup>32, 33</sup> and there is potential to extend the measurement approach to infer reaction rate coefficients. Along these lines, here we develop an IM-MS method to examine nano-ion-neutral reaction kinetics, and employ it with a differential mobility analyzer-mass spectrometer (DMA-MS) for the characterization of  $C_{60}^-$  ozonation reactions, considering both single ( $n = 1$ ) and multiple ( $n > 1$ ) reactions of the form:



The formation of fullerene epoxides ( $C_{60}O_n$ ) by fullerene photo-oxidation and ozonation has been observed in several previous studies.<sup>34, 35</sup> However, epoxide nano-ion formation via ozonation of isolated gas phase fullerene nano-ions has only been reported in the literature in one previous study,<sup>36</sup> and attempts have not been made to infer reaction rate kinetics. The method we implement builds upon prior selected ion flow tube (SIFT)<sup>10-13, 37</sup> and IM-MS efforts<sup>38-40</sup> to infer reaction rate coefficients for smaller (sub 100 Da) ions and for  $C_{60}$  cations. It is directly implementable on a wide variety of low-field IM-MS instruments, without the need for significant instrument modification, and can yield reaction rate coefficients at atmospheric pressure. The IM-MS method can additionally be applied to a variety of nano-ions, including biomolecular ions. Our results in studying  $C_{60}^-$  reactivity yield the reaction rate coefficients for the addition of up to 5 oxygen atoms via ozonation, with additional characterization of the evolution of the rate coefficient for up to 16 added oxygen atoms on average.

## EXPERIMENTAL METHODS

A depiction of the measurement system is shown in Figure 1, with a more detailed schematic diagram provided in the supporting information.  $C_{60}$  powder (99.5%, Sigma-Aldrich)

was placed in a ceramic tube within a furnace (Lindbergh Blue) that was set at 550-560 °C. A carrier gas ( $1.7 \text{ l min}^{-1} \text{ N}_2$ ) was sent into the furnace entraining the vaporized  $\text{C}_{60}$  molecules.<sup>41</sup> The flow exited the tube furnace and subsequently entered an ionization chamber, which contained a Po-210 radioactive source. Alpha particle emission from Po-210 yields roughly equal concentrations of positive and negative ions (typically from trace impurities in gases).<sup>42</sup>  $\text{C}_{60}$  molecules, due to their strong electron affinity, became negatively charged  $\text{C}_{60}^-$  anions through this process.<sup>43</sup> The Po-210 ionization source was mounted directly on the front plate of the differential mobility analyzer (parallel plate DMA P5, SEADM).  $1 \text{ l min}^{-1}$  of the flow was withdrawn from the chamber via a vacuum pump, while the remaining  $0.7 \text{ l min}^{-1}$  was sent into the DMA. To facilitate the transmission of  $\text{C}_{60}^-$  into the DMA, a voltage of  $-1000 \text{ V}$  (relative to the DMA inlet) was applied to one end of ionization chamber, hence ion transmission was driven both fluid mechanically and electrostatically.

$\text{C}_{60}^-$  ions and their ozonation products were classified by ion mobility in the DMA. The DMA was operated with a recirculating sheath flow pumped by a vacuum blower; ports on the sheath flow lines were connected to ozone sources. The ozone concentration within the DMA sheath flow was modulated, and  $\text{C}_{60}^-$  anions were only exposed to ozone during their transit through DMA. To adjust ozone concentrations, both a UV ozone generator (Model OG-2, UVP, Upland, CA) and a corona discharge ozone generator (Model A2ZS-32G Lab Ozone Generator, A2Z Ozone Inc.) were employed. The flow exiting the ozone generators was diluted by  $4 \text{ l min}^{-1}$  of nitrogen.  $3.3 \text{ l min}^{-1}$  of the combined flow of  $\text{N}_2$  and the ozone laden oxygen was pulled into the DMA sheath loop. A total of  $4 \text{ l min}^{-1}$  was continuously drawn from the DMA recirculating loop into vacuum pumped mass flow controller ( $3.3 \text{ l min}^{-1}$  from the ozone generator and dilution flow, and  $0.7 \text{ l min}^{-1}$  of the  $\text{C}_{60}^-$  laden inlet flow). Prior to entering the mass flow

controller, the flow was split, with  $1.45 \text{ l min}^{-1}$  going through an ozone analyzer (Thermal Environmental 49C). A stable reading on the ozone analyzer indicated the ozone concentrations in the DMA were steady; for each measurement, stabilization required 0.5 - 2 h after ozone generation began. Because of the high sheath flow rate in the DMA and the low concentrations of ions (relative to ozone), we assume that the ozone concentration in the DMA was constant across the entire sheath flow line. By using both ozone generators we were able to vary the equilibrium ozone mixing ratio within the DMA loop from  $10^1$  ppb to  $10^5$  ppb (by number concentration).

Like drift tube ion mobility spectrometers (and not to be confused with similarly named differential ion mobility spectrometers), DMAs are linear mobility spectrometers which operate at relatively low Townsend values (i.e. in the low field limit). In this study, the electric field strength within the DMA was less than  $2500 \text{ V cm}^{-1}$  for all measurements ( $< 10 \text{ Td}$ ), and ions traversing the DMA had speeds of order  $10^1 \text{ m s}^{-1}$ , well below the mean thermal speeds of the sheath gas molecules. Therefore, ion heating during the measurement was negligible, as ion-neutral relative kinetic energy distributions were near Maxwell-Boltzmann distributed about the sheath gas temperature. The temperature of the DMA sheath flow was controlled by a water jacket heat exchanger at  $295 \pm 0.5 \text{ K}$  for all experiments. Distinct from drift tubes, DMAs are fixed residence time instruments. The residence time is the ratio of the distance from the DMA inlet to the outlet in the streamwise direction to sheath flow velocity, hence it is adjustable by adjusting the sheath flow rate. For the settings employed, the residence time of the transmitted ions in the DMA was 0.48 ms. As the sheath flow rate was not directly measurable, this residence time was determined by measuring the DMA transmission voltage of known mobility tetraheptylammonium<sup>+</sup> (THA<sup>+</sup>) ions<sup>44</sup> ( $\sim 2150 \text{ V}$  with a 1 cm gap from inlet to outlet).

Measurement of  $\text{THA}^+$  mobility spectrum also yielded the DMA resolution ( $\sim 40$ ); the resolution in mobility is identical to the resolution in residence time. At the beginning of each set of experiments, the mobility spectrum of  $\text{C}_{60}^-$  (without ozonation) was also collected as system calibration to ensure that the ion residence time remained unchanged from day to day. The mobility of  $\text{C}_{60}^-$  varied within  $\pm 2.5\%$  among all experiments and is shown in the supporting information in relation to the  $\text{THA}^+$  ion mobility spectrum.

The DMA was interfaced with a QSTAR XL mass spectrometer (MD Sciex), with the time-of-flight section utilized for mass analysis.<sup>25, 45</sup> We collected two dimensional mobility-mass spectra, for which the voltage difference across the DMA electrodes was stepped in 10 V increments in the 1800-2500 V range, with the mass spectrometer measuring in a mass range of 30-3000 Th. Inlet declustering potentials and focusing potentials of the mass spectrometer were set to minimum values to preserve the integrity of ozonation products.

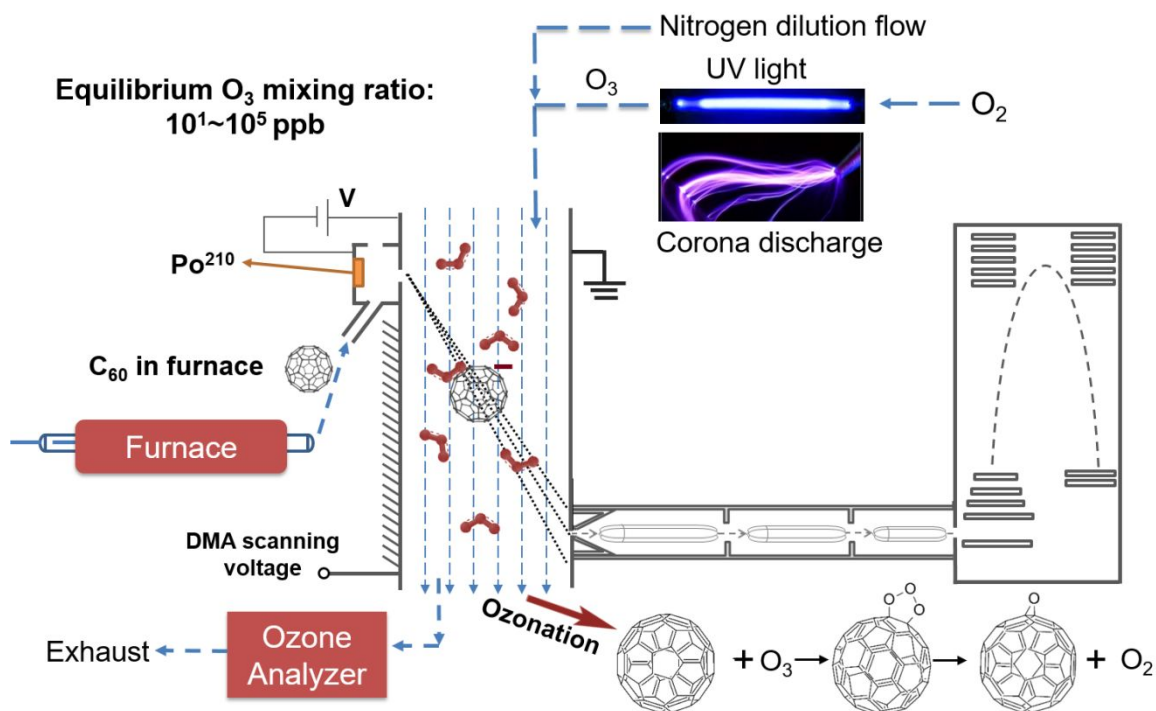


**Figure 1.** A depiction of the DMA-MS experimental setup. The reaction mechanism of the first oxygen addition, leading to fullerene epoxide formation, is also shown in the bottom-right.

## RESULTS & DISCUSSION

In total, DMA-MS experiments yielded the mobility-mass distributions for ozonation products with controlled, sub-millisecond exposure time to a controlled concentration of ozone. Two dimensional mass-mobility contour plots are shown in Figures 2a-c for ozone mixing ratios of 154 ppb, 980 ppb and 71.5 ppm, respectively. Along the  $m/z$  axis, starting from  $m/z = 720$  ( $C_{60}^-$ ), a clear separation of 16 Th emerged between mass peaks, indicating oxygen atom addition. Ions with more oxygen atoms added had decreased apparent mobilities, as they were transmitted at higher voltages. All plots reveal first increasing and then decreasing peak widths in the mobility dimension with increasing levels of oxidation. This is expected for irreversible reactions occurring during migration through the DMA; the mobility spectrum for a given  $m/z$  value is a convolution of linear combinations of the parent and product ions mobilities, where the combinations are weighted by the fraction of time the detected ion spends as each parent or product.<sup>25</sup> The apparent mobility of intermediate product ions hence shifts modestly with changing ozone concentration.

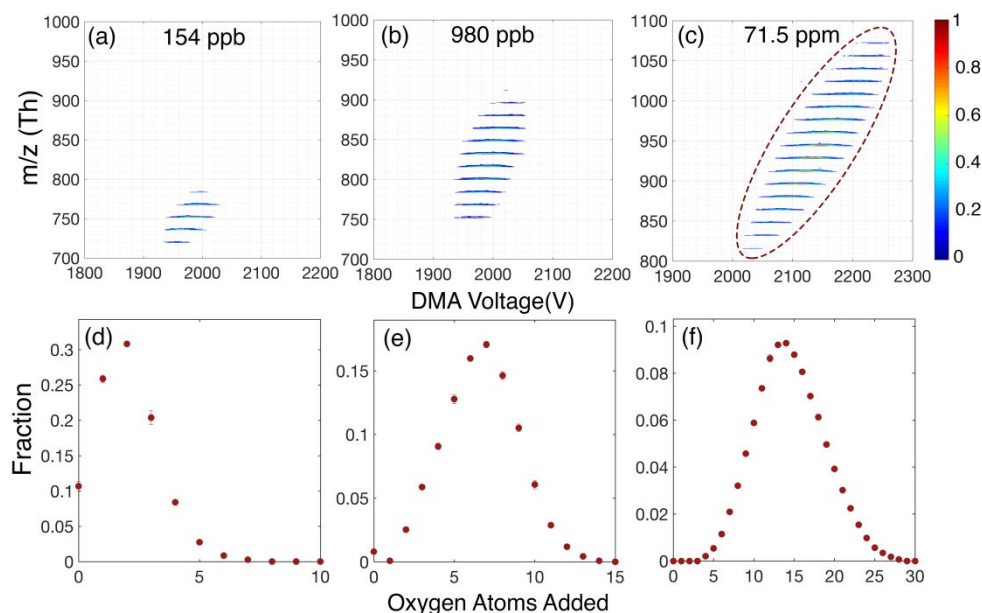
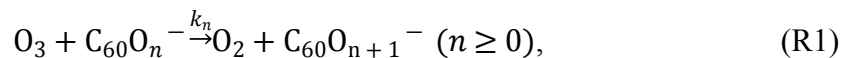


**Figure 2.** Mobility-mass spectra (a-c) for three different  $O_3$  concentrations and corresponding fraction ratios of different oxidation states of  $C_{60}O_m^-$  ions.

While it is possible to utilize the apparent mobility distributions to obtain information about reaction kinetics, quantification using this information alone is difficult in instances where there are multiple, sequential reactions occurring. More direct information on reaction rate kinetics is provided by the signal intensities of product ions measured by the mass spectrometer. Figures 2d-f display the corresponding oxygen addition distribution for selected ozone mixing ratios. In these plots, alternating signal intensities, which would be indicative of  $O_3$  physisorption, or chemical reactions that lead to addition of multiple oxygen atoms to the parent ions, did not emerge for any ozone mixing ratio. This suggests that oxygen atoms were added sequentially through reaction with ozone. In addition, at an ozone mixing ratio of 71.5 ppm, addition of up to 28 oxygen atoms was observed with an average oxygen addition near 14. These highly oxidized reaction products are anticipated, as they were previously observed by corona discharge ionization of  $C_{60}$  in an oxygen rich environment,<sup>36</sup> with oxygen content much higher than those obtained in liquid phase  $C_{60}$  ozonation.<sup>35, 46, 47</sup>

We employ a sequential oxygen addition model for reaction rate inference from measurements. We assumed that single oxygen atoms were incorporated into the nano-ion  $C_{60}O_n^-$  via reactions of the type:



where  $k_n$  is the reaction rate constant (reported on a number concentration basis). The formation of Criegee intermediates is implicitly assumed as an intermediate step (not shown). This model leads to a set of first order linear equations that describe the evolution of the product ion distribution. To obtain the reaction rates  $k_n$ , we fit the model prediction to experimental oxygen addition distributions (similar to those that are shown in Figure 2d-f) by varying the values of  $k_n$  for  $n=0-4$ . We remark that for the sequential addition model proposed, the distribution of nano-ions containing 0 to  $m$  oxygen atoms ( $C_{60}O_{0\sim m}^-$ ) only depends on the rate coefficients from  $k_0$  to  $k_m$ . We first calculated the optimal  $k_0$  by minimizing the deviation between model predicted and experimentally observed  $C_{60}O^-$  signal intensity fractions (the ratio of  $C_{60}O^-$  ion signal intensity to all  $C_{60}O_{0\sim m}^-$  ion signal intensities combined) using a least square criterion. In this process,  $C_{60}O^-$  signal intensity fractions measured at ozone mixing ratios less than 980 ppb were utilized. Data obtained at higher ozone concentrations were excluded because secondary reactions, which are not included in the sequential addition model, become important with increasing ozone concentrations (discussed subsequently). With the optimal  $k_0$  determined, we then calculated  $k_1$ , using observed  $C_{60}O^-$  signal intensity fractions at ozone mixing ratios up to 980 ppb. This process was iterated until  $k_4$  was determined, with the values of  $k_0$  to  $k_4$  inferred as follows:  $k_0 = 1.17 \times 10^{-9} \text{ cm}^3 \text{ s}^{-1}$ ,  $k_1 = 1.08 \times 10^{-9} \text{ cm}^3 \text{ s}^{-1}$ ,  $k_2 = 8.95 \times 10^{-10} \text{ cm}^3 \text{ s}^{-1}$ ,  $k_3 = 7.51 \times 10^{-10} \text{ cm}^3 \text{ s}^{-1}$  and  $k_4 = 6.94 \times 10^{-10} \text{ cm}^3 \text{ s}^{-1}$ . We estimate the uncertainties of  $k_0$  to be  $\pm 4.5\%$ . This was determined by incorporating the uncertainties of residence time ( $\pm 3.5\%$ ,

$\pm 2.5\%$  from finite instrument resolution and  $\pm 2.5\%$  from day to day variation) and uncertainties of ozone concentration ( $\pm 2.0\%$ ) into the sequential addition model and recalculating  $k_0$ . The uncertainties of  $k_n$  increase with  $n$  since errors propagate. We did not calculate the values of  $k_{\geq 5}$ , both because of error propagation and because of secondary reactions that can interfere with measurements of  $C_{60}O_{\geq 5}^-$ . Incorporating  $k_0$  to  $k_4$  into the sequential model, we calculated the model predicted oxygen addition distribution, which were compared with experimental measured distributions in Figure 3a.

It is informative to compare  $k_0$  with the collision rate between ozone molecules and  $C_{60}^-$  ions. Taking into account of ion-dipole interaction,<sup>48</sup> the gas phase collision rate between  $O_3$  and  $C_{60}^-$  is estimated to be near  $k_{coll} = 3.27 \times 10^{-9} \text{ cm}^3 \text{ s}^{-1}$  (see the supporting information for details), which is of the same order of magnitude as  $k_0$ . This  $k_0$  is also orders of magnitude higher than reaction rates typically observed between ozone and electrically neutral organic compounds that contain double bonds (e.g. isoprene<sup>49</sup> and monoterpenes<sup>50</sup>), suggesting ozonation of graphene based materials occurs rapidly in atmospheric pressure environments. Reaction rate coefficients close to the collision controlled limit were observed previously for  $C_{60}$  cations with amines via SIFT;<sup>13</sup> this similar finding supports both the use IM-MS in nano-ion reaction rate investigation and our finding that ozonation of  $C_{60}^-$  occurs rapidly.

We further propose a simple rate coefficient equation to approximately describe the evolution of fullerene epoxide nano-ions. The average oxygen addition is displayed as crimson points as a function of ozone mixing ratio in figure 3b. The error bar for each data point indicates the standard deviation of the number of oxygen atoms added (i.e. the standard deviation of the distributions shown in Figure 3d-f). We assume  $k_n$  decays exponentially via the relationship:

$$k_n = k_0 \exp(-\theta n), \quad n = 0, 1, 2, \dots, 30. \quad (1)$$

Using the equation (1), we can calculate the average oxygen atoms added to fullerene at any ozone concentration. Fitting to all results led to  $\theta = 0.4$  and  $k_0 = 1.17 \times 10^{-9} \text{ cm}^3 \text{ s}^{-1}$ . The resulting average number of oxygen atoms predicted via equation (1) is plotted as a dashed line in Figure 3b. Overall, predictions based upon equation (1) agree well with measurements. However, the  $\theta = 0.4$  based rate constants for the low  $n$  values are lower than those determined via sequential fitting, and  $\theta = 0.4$  is only applicable at the measurement temperature of 295 K (though one could expect equation 1 to be extrapolated to other temperatures as an Arrhenius-like expression). The decrease of reaction rates is likely attributable to the decreased number of double bonds available for reaction, as well as stronger steric effects as more oxygen atoms are added to the nano-ion surface.

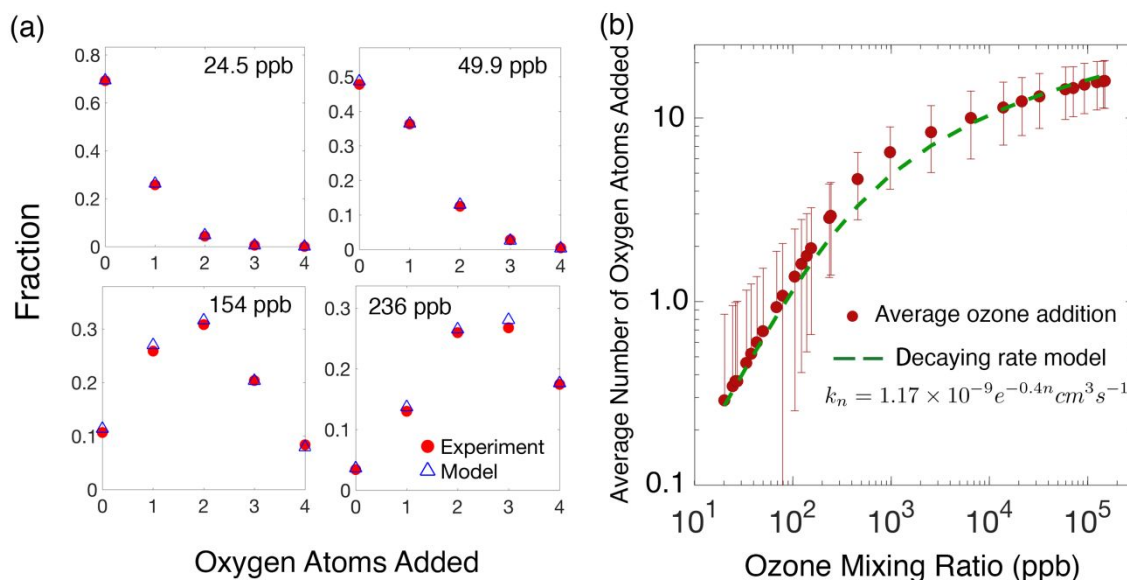


**Figure 3.** (a) Comparison of the oxygen addition distribution from experiments and model predictions. The rate coefficients used in the model ( $k_{0-4}$ ) were obtained by the fitting procedure explained in text, leading to the following values:  $k_0 = 1.17 \times 10^{-9} \text{ cm}^3 \text{ s}^{-1}$ ,  $k_1 = 1.08 \times 10^{-9} \text{ cm}^3 \text{ s}^{-1}$ ,  $k_2 = 8.95 \times 10^{-10} \text{ cm}^3 \text{ s}^{-1}$ ,  $k_3 = 7.51 \times 10^{-10} \text{ cm}^3 \text{ s}^{-1}$  and  $k_4 = 6.94 \times 10^{-10} \text{ cm}^3 \text{ s}^{-1}$ . (b) Oxygen addition as a function of ozone mixing ratio. Data in crimson are from experiments, and the spread indicates the standard deviation for the number oxygen atoms

incorporated into product ions. Model predicted average oxygen addition with equation 1 is shown as a green dashed curve.

In addition to  $C_{60}O_n^-$ , we observed  $m/z$  peaks corresponding to  $C_{60}O_n^- + 4$  Da,  $C_{60}O_n^- + 8$  Da,  $C_{60}O_n^- + 12$  Da and  $C_{60}O_n^- + 14$  Da (local intensity maxima of the mass spectra are provided in Figure S3 of the supporting information). The peak series of  $C_{60}O_n^- + 4$  Da had the highest intensity among these; its intensity relative to that of  $C_{60}O_n^-$  increased with ozone concentration, as is shown in Figure 4. At low ozone mixing ratio, signal intensities of  $C_{60}O_n^- + 4$  Da were negligible, while at high ozone mixing ratios (e.g. 193ppm), intensities of  $C_{60}O_n^- + 4$  Da can reach ~20% of  $C_{60}O_n^-$ . It is likely that the additional peaks  $C_{60}O_n^- + 4$  Da,  $C_{60}O_n^- + 8$  Da and  $C_{60}O_n^- + 12$  Da originated from CO and/or CO<sub>2</sub> loss by highly oxidized ions. This is supported by prior studies where such dissociation in  $C_{60}O_3$  was facilitated by laser induced fragmentation and collision induced dissociation.<sup>51</sup> The formation mechanism for the  $C_{60}O_n^- + 14$  Da is currently unclear. It is possible that the trace amount of water or other contaminants within the DMA sheath flow line participated in reactions, leading to the incorporation of atoms other than oxygen into the reaction products. The lack of exact mass level resolution in the mass spectrometer employed prevented clear chemical identification of these ions. Examination of the mobility spectra of the additional peaks also suggests that CO/CO<sub>2</sub> loss occurs within the DMA. The mobilities of these ions do not align exactly with any  $C_{60}O_n^-$  ions, indicating that these peaks do not originate from dissociation within the mass spectrometer.

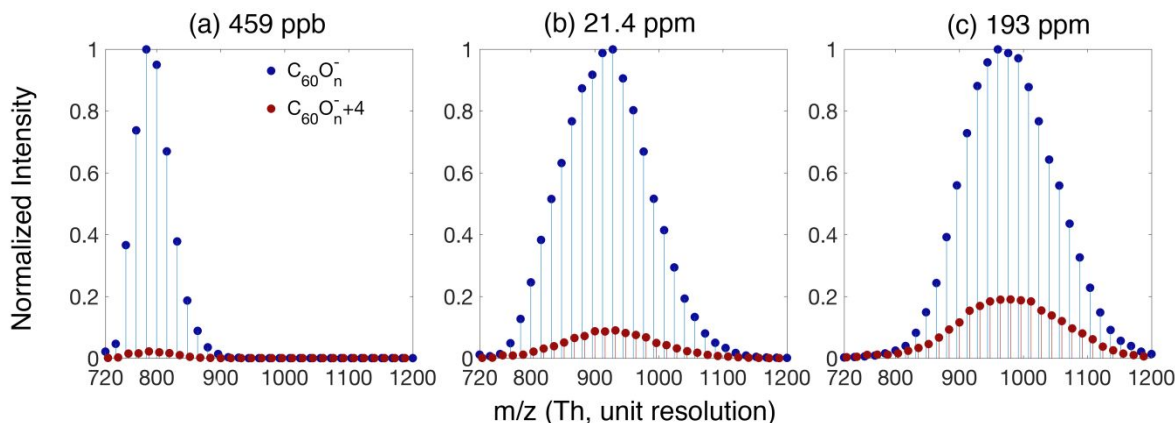


**Figure 4.** Comparison of signal intensities from  $C_{60}O_n^{-+4}$  to those from  $C_{60}O_n^{-}$  at 3 ozone mixing ratios. The ion intensities were normalized by highest ion intensity within for a given ozone mixing ratio.

## CONCLUSIONS

We demonstrate for the first time the potential use of DMAs as controlled residence time ion-neutral reaction cells. By controlling the ozone concentration in the DMA, we were able to determine multiple reaction rates for  $C_{60}O_n^{-}$  oxygenation assuming oxygen atoms were added sequentially. It was found that an exponentially decaying reaction rate can explain the average oxygen addition well. Mass peaks other than  $C_{60}O_n^{-}$  were identified, which can be attributed to CO or CO<sub>2</sub> loss from the highly oxidized reaction products. The method employed in this study, i.e. using IM-MS instruments to study gas phase ion-vapor reactions, can potentially be applied to study the gas phase reactivity of other ions of scientific interest, including but not limited to proteins,<sup>52, 53</sup> nucleic acids,<sup>54</sup> polymers,<sup>55</sup> and atmospheric clusters,<sup>56, 57</sup> all of which have been analyzed previously through more typically IM-MS implementation. In principle, it can additionally be extended to examine the kinetics of ozonolysis reactions<sup>58, 59</sup> and similar, multiple product reactions in the gas phase. Future studies comparing DMA based reaction rate constants to alternative measurement approaches will be needed to assess potential of the DMA based method for a wide variety of ion-neutral reactions. While DMAs are extremely well suited

to be controlled residence time reaction cells, the measurement approach can be extended to other linear ion mobility spectrometers. The only requirements for implementation are independent control over residence time and reactant gas concentration in the ion mobility cell, which is certainly met by not only differential mobility analyzers but also trapped ion mobility spectrometers.<sup>27</sup> Although this is not strictly the case for drift tube ion mobility spectrometers, reaction rate kinetics could nonetheless be determined using drift tubes modifying the analysis approach to account for variable residence times.

## **SUPPORTING INFORMATION**

A detailed depiction of the experimental setup, the mobility spectra for  $\text{THA}^+$  and  $\text{C}_{60}^-$ , method of calculation for the collision rate between  $\text{C}_{60}^-$  and  $\text{O}_3$ , mass peaks at high ozone mixing ratio are available online.

## **ACKNOWLEDGMENTS**

This work was supported by was supported by US Department of Energy Award DE-SC0018202. The authors thank Dr. Kenjiro Iida (National Institute of Advanced Industrial Science and Technology, Tsukuba, Japan) for guidance on the generation of isolated  $\text{C}_{60}$  in the gas-phase via evaporation in a furnace.

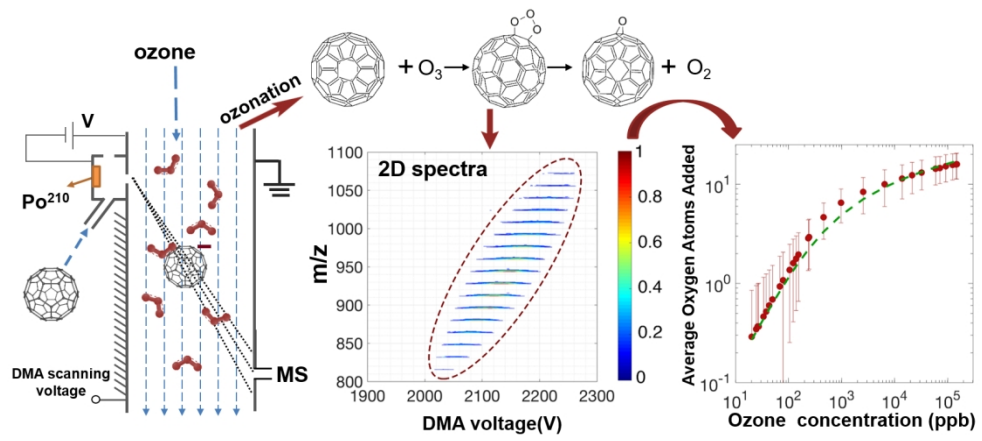
## REFERENCES

1. A. M. Rao, P. Zhou, K.-A. Wang, G. T. Hager, J. M. Holden, Y. Wang, W. T. Lee, X.-X. Bi, P. C. Eklund, D. S. Cornett, M. A. Duncan and I. J. Amster, *Science*, 1993, **259**, 955-957.
2. F. Giacalone and N. Martín, *Chemical Reviews*, 2006, **106**, 5136-5190.
3. L. Echegoyen and L. E. Echegoyen, *Accounts of Chemical Research*, 1998, **31**, 593-601.
4. Y. Matsuo, J. Kawai, H. Inada, T. Nakagawa, H. Ota, S. Otsubo and E. Nakamura, *Advanced Materials*, 2013, **25**, 6266-6269.
5. Y. Matsuo, K. Ogumi, Y. Zhang, H. Okada, T. Nakagawa, H. Ueno, A. Gocho and E. Nakamura, *Journal of Materials Chemistry A*, 2017, **5**, 2774-2783.
6. P. Strobel, J. Ristein and L. Ley, *The Journal of Physical Chemistry C*, 2010, **114**, 4317-4323.
7. A. J. Tiwari, J. R. Morris, E. P. Vejerano, M. F. Hochella and L. C. Marr, *Environmental Science & Technology*, 2014, **48**, 2706-2714.
8. R. Dattani, K. F. Gibson, S. Few, A. J. Borg, P. A. DiMaggio, J. Nelson, S. G. Kazarian and J. T. Cabral, *Journal of Colloid and Interface Science*, 2015, **446**, 24-30.
9. D. Heymann and R. B. Weisman, *Comptes Rendus Chimie*, 2006, **9**, 1107-1116.
10. V. Baranov, J. Wang, G. Javahery, S. Petrie, A. C. Hopkinson and D. K. Bohme, *Journal of the American Chemical Society*, 1997, **119**, 2040-2049.
11. S. Petrie, G. Javahery, J. Wang and D. K. Bohme, *Journal of the American Chemical Society*, 1992, **114**, 9177-9181.
12. V. Baranov, A. C. Hopkinson and D. K. Bohme, *Journal of the American Chemical Society*, 1997, **119**, 7055-7060.
13. G. Javahery, S. Petrie, H. Wincel, J. Wang and D. K. Bohme, *Journal of the American Chemical Society*, 1993, **115**, 5716-5722.
14. T. P. Martin, U. Näher, H. Schaber and U. Zimmermann, *Physical Review Letters*, 1993, **70**, 3079-3082.
15. C. Yeretian, K. Hansen, F. Diederichi and R. L. Whetten, *Nature*, 1992, **359**, 44.
16. H. Wang, *Proceedings of the Combustion Institute*, 2011, **33**, 41-67.
17. K. O. Johansson, T. Dillstrom, P. Elvati, M. F. Campbell, P. E. Schrader, D. M. Popolan-Vaida, N. K. Richards-Henderson, K. R. Wilson, A. Violi and H. A. Michelsen, *Proceedings of the Combustion Institute*, 2017, **36**, 799-806.
18. G. von Helden, M. T. Hsu, P. R. Kemper and M. T. Bowers, *The Journal of Chemical Physics*, 1991, **95**, 3835-3837.
19. E. C. Tyo and S. Vajda, *Nature Nanotechnology*, 2015, **10**, 577.

20. M. F. Jarrold, *Science*, 1991, **252**, 1085-1092.
21. M. F. Jarrold, Y. Ijiri and U. Ray, *The Journal of Chemical Physics*, 1991, **94**, 3607-3618.
22. J. C. May, C. R. Goodwin, N. M. Lareau, K. L. Leaptrot, C. B. Morris, R. T. Kurulugama, A. Mordehai, C. Klein, W. Barry, E. Darland, G. Overney, K. Imatani, G. C. Stafford, J. C. Fjeldsted and J. A. McLean, *Analytical Chemistry*, 2014, **86**, 2107-2116.
23. K. A. Servage, J. A. Silveira, K. L. Fort and D. H. Russell, *Accounts of chemical research*, 2016, **49**, 1421-1428.
24. K. A. Morrison, W. F. Siems and B. H. Clowers, *Analytical Chemistry*, 2016, **88**, 3121-3129.
25. C. J. Hogan and J. Fernandez de la Mora, *Physical Chemistry Chemical Physics*, 2009, **11**, 8079-8090.
26. S. D. Pringle, K. Giles, J. L. Wildgoose, J. P. Williams, S. E. Slade, K. Thalassinou, R. H. Bateman, M. T. Bowers and J. H. Scrivens, *International Journal of Mass Spectrometry*, 2007, **261**, 1-12.
27. K. Michelmann, J. A. Silveira, M. E. Ridgeway and M. A. Park, *Journal of The American Society for Mass Spectrometry*, 2015, **26**, 14-24.
28. C. Laphorn, F. Pullen and B. Z. Chowdhry, *Mass Spectrometry Reviews*, 2013, **32**, 43-71.
29. J. D. Eschweiler, A. T. Frank and B. T. Ruotolo, *Journal of The American Society for Mass Spectrometry*, 2017, **28**, 1991-2000.
30. C. Li and C. J. Hogan, *Aerosol Science and Technology*, 2017, **51**, 653-664.
31. D. Oberreit, V. K. Rawat, C. Larriba-Andaluz, H. Ouyang, P. H. McMurry and C. J. Hogan, *The Journal of Chemical Physics*, 2015, **143**, 104204.
32. P. Kwantwi-Barima, C. J. Hogan and B. H. Clowers, *The Journal of Physical Chemistry A*, 2019, **123**, 2957-2965.
33. P. Kwantwi-Barima, H. Ouyang, C. J. Hogan and B. H. Clowers, *Analytical Chemistry*, 2017, **89**, 12416-12424.
34. K. M. Creegan, J. L. Robbins, W. K. Robbins, J. M. Millar, R. D. Sherwood, P. J. Tindall, D. M. Cox, J. P. McCauley and D. R. Jones, *Journal of the American Chemical Society*, 1992, **114**, 1103-1105.
35. J.-P. Deng, C.-Y. Mou and C.-C. Han, *Fullerene Science and Technology*, 1997, **5**, 1033-1044.
36. H. Tanaka, K. Takeuchi, Y. Negishi and T. Tsukuda, *Chemical Physics Letters*, 2004, **384**, 283-287.

37. G. I. Mackay, G. D. Vlachos, D. K. Bohme and H. I. Schiff, *International Journal of Mass Spectrometry and Ion Physics*, 1980, **36**, 259-270.
38. K. Giles and E. P. Grimsrud, *The Journal of Physical Chemistry*, 1992, **96**, 6680-6687.
39. K. Giles and E. P. Grimsrud, *The Journal of Physical Chemistry*, 1993, **97**, 1318-1323.
40. A. J. Bell, K. Giles, S. Moody and P. Watts, *International Journal of Mass Spectrometry and Ion Processes*, 1998, **173**, 65-70.
41. H. Tanaka and K. Takeuchi, *Applied Physics A*, 2005, **80**, 759-761.
42. A. Maißer, J. M. Thomas, C. Larriba-Andaluz, S. He and C. J. Hogan Jr, *Journal of Aerosol Science*, 2015, **90**, 36-50.
43. G. Chen, R. G. Cooks, E. Corpuz and L. T. Scott, *Journal of the American Society for Mass Spectrometry*, 1996, **7**, 619-627.
44. S. Ude and J. Fernández de la Mora, *Journal of Aerosol Science*, 2005, **36**, 1224-1237.
45. J. Rus, D. Moro, J. A. Sillero, J. Royuela, A. Casado, F. Estevez-Molinero and J. Fernández de la Mora, *International Journal of Mass Spectrometry*, 2010, **298**, 30-40.
46. R. Malhotra, S. Kumar and A. Satyam, *Journal of the Chemical Society, Chemical Communications*, 1994, 1339-1340.
47. Y. Tajima and K. Takeuchi, *The Journal of Organic Chemistry*, 2002, **67**, 1696-1698.
48. T. Su and M. T. Bowers, *Journal of the American Chemical Society*, 1973, **95**, 7609-7610.
49. V. G. Khamaganov and R. A. Hites, *The Journal of Physical Chemistry A*, 2001, **105**, 815-822.
50. D. J. Stewart, S. H. Almagro, J. P. Lockhart, O. M. Mohamed, D. R. Nutt, C. Pfrang and G. Marston, *Atmospheric Environment*, 2013, **70**, 227-235.
51. S. G. Penn, D. A. Costa, A. L. Balch and C. B. Lebrilla, *International Journal of Mass Spectrometry and Ion Processes*, 1997, **169-170**, 371-386.
52. M. F. Bush, Z. Hall, K. Giles, J. Hoyes, C. V. Robinson and B. T. Ruotolo, *Analytical Chemistry*, 2010, **82**, 9557-9565.
53. C. J. Hogan and J. Fernandez de la Mora, *Journal of the American Society for Mass Spectrometry*, 2011, **22**, 158-172.
54. R. Ferreira, A. Marchand and V. Gabelica, *Methods*, 2012, **57**, 56-63.
55. C. Larriba, J. Fernandez de la Mora and D. E. Clemmer, *Journal of the American Society for Mass Spectrometry*, 2014, **25**, 1332-1345.
56. J. M. Thomas, S. He, C. Larriba-Andaluz, J. W. DePalma, M. V. Johnston and C. J. Hogan, *Physical Chemistry Chemical Physics*, 2016, **18**, 22962-22972.
57. L. Ahonen, C. Li, J. Kubečka, S. Iyer, H. Vehkamäki, T. Petäjä, M. Kulmala and C. J. Hogan, *The Journal of Physical Chemistry Letters*, 2019, **10**, 1935-1941.

58. M. C. Thomas, T. W. Mitchell and S. J. Blanksby, *Journal of the American Chemical Society*, 2006, **128**, 58-59.
59. B. L. Poad, X. Zheng, T. W. Mitchell, R. D. Smith, E. S. Baker and S. J. Blanksby, *Analytical Chemistry*, 2017, **90**, 1292-1300.



296x130mm (150 x 150 DPI)